*Geol. Mag.* **147** (*2*), *2010, pp. 219–232.* © *Cambridge University Press 2009*
doi:10.1017/S0016756809990367


# Petrogenesis and tectonic implications of Late Mesozoic granites in the NE Yangtze Block, China: further insights from the Jiuhuashan–Qingyang complex

XI-SHENG XU*†, KAZUHIRO SUZUKI‡, LEI LIU* & DE-ZI WANG*

*State Key Laboratory for Mineral Deposits Research, Department of Earth Sciences, Nanjing University, Nanjing 210093, China
‡Center for Chronological Research, Nagoya University, Nagoya 464-8602, Japan

(*Received* 9 March 2009; *accepted* 3 June 2009; First published online 27 October 2009)

**Abstract –** The Jiuhuashan–Qingyang complex is one of the Mesozoic granite complexes in the NE Yangzte Block, China. New petrographical and petrochemical data show that the complex comprises a dominant granodiorite–monzogranite, the Qingyang body, which was intruded by the Jiuhuashan granite body. The two are characterized by distinct mineral components and trace element patterns. Compared to the Qingyang granodiorite and monzogranite, the Jiuhuashan granite is enriched in Rb, Th, U, Nb, Ta, Hf, Yb and Lu, and depleted in Ba, Sr, Nd, Sm, Eu, Gd and Ti, which are ascribable to the separation of plagioclase and biotite, and crystallization of thorite and fergusonite during the magmatism. New LA-ICPMS zircon U–Pb dating suggests that the crystallization age of the Qingyang body is 139–133 Ma, and the Jiuhuashan granite followed at 127 Ma. Moreover, the new zircon U–Pb dates reveal that Archaean materials were involved in the formation of these magmas, and that a sodium-rich metasomatic event occurred at about 100 Ma. The CHIME monazite and zircon ages studied for the Jiuhuashan body agree well with the LA-ICPMS zircon ages. Integrating this information with previous studies for granites in the NE Yangtze Block and in the coastal area of SE China, we believe that all of these Late Mesozoic granites were produced under the tectonic regime of palaeo-Pacific plate subduction towards the SE China continent in a NW direction, but the granites in the NE Yangtze Block are basically derived by crustal melting with limited mixing of juvenile material during the magma generation.

Keywords: granite complex, petrochemistry, zircon U–Pb age, CHIME age, SE China.

## 1. Introduction

The South China Block and North China Block were sutured in the late Middle Triassic to Middle Jurassic period along the Qinling–Dabie and Sulu orogen (Zhang *et al.* 1985, 2000; Li, 1998; Grimmer *et al.* 2003; Wang *et al.* 2007). The South China Block can be subdivided into two blocks: the Yangtze Block to the NW and the Cathaysia Block to the SE, which were connected by collision during the Proterozoic Grenvillian orogen (Charvet *et al.* 1996; Li, 1998) (Fig. 1a). The Mesozoic granite-volcanic rocks are widely distributed in the South China Block. These rocks occurred in different ages within the Mesozoic, with complex formation processes and close affinity with mineralization of W, Sn, U, Nb–Ta, etc. The Indosinian granites (210–250 Ma) are distributed inland, while the dominant Yanshanian granites (180–90 Ma) are distributed in the southeast of the South China Block. The Late Yanshanian granite-volcanic (140–90 Ma) rocks occupy about 139 920 km$^2$, are genetically associated with active continental margin magmatism, and are distributed mostly in the coastal region (Fig. 1a). However, previous Mesozoic tectono-magmatism studies have concentrated on the southeast; the contemporaneous granites in the NE Yangtze Block (Yangzte foldbelt) deserve further study. The Yangtze foldbelt (Fig. 1a) strikes NE, and the stratified bedrock of this foldbelt comprises late Precambrian sedimentary and metamorphic rocks and Early Palaeozoic sandstone. The age of the basement beneath this foldbelt is uncertain, but Indosinian (Triassic period) and Yanshanian (Jurassic to Cretaceous period) thermal overprints have been identified (Yuan *et al.* 2003, 2006). The Yanshanian intermediate to silicic intrusions exposed in this foldbelt have been subdivided into several zones by Chen *et al.* (1993), for example, diorite–quartz diorite–granodiorite stocks along the Yangtze River, mostly associated with Cu, Fe and Au mineralization (the Yangtze zone), granodiorite–granite batholiths or large stocks further south and away from the Yangtze River (the Jiangnan zone).

Based on Sr–Nd isotopic analysis of the intrusions, Chen, Zhou & Foland (1985) and Chen *et al.* (1993) argued that (a) the granitoids of Jiangnan zone were formed by crustal anatexis and no mantle magmas were directly involved during the magmatism, (b) the isotopic characteristics of the intrusions are very similar to the nearby Proterozoic metamorphic rocks

†Author for correspondence: xsxu@nju.edu.cn

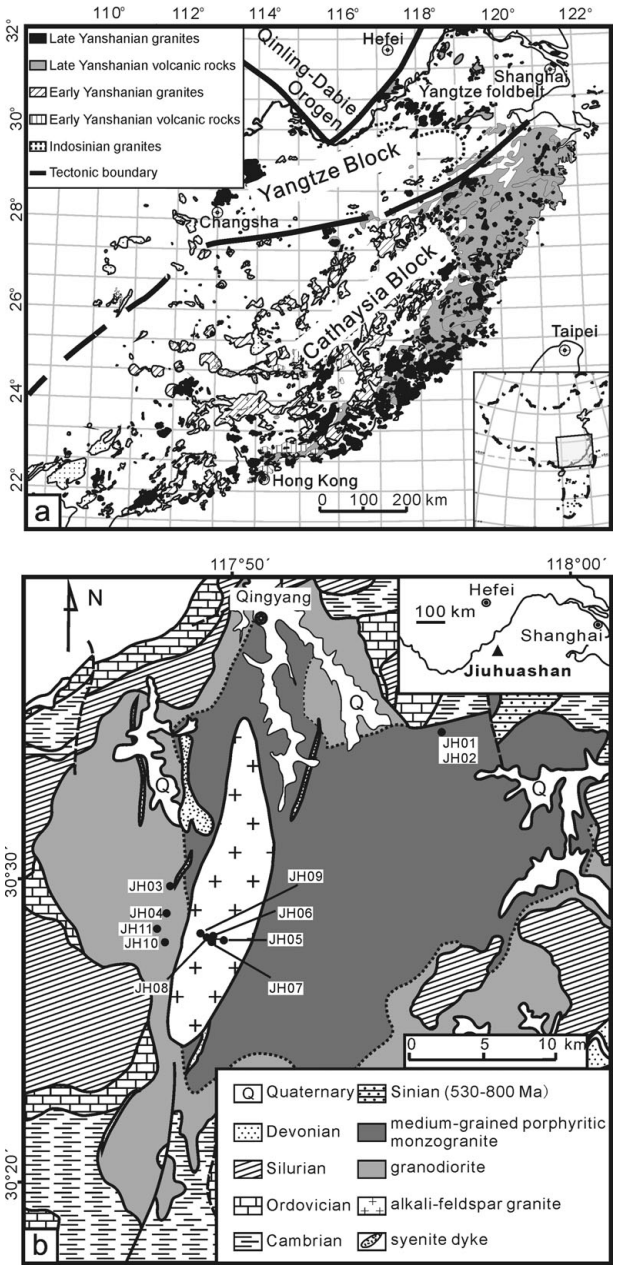


Figure 1. (a) Distribution of Mesozoic granite-volcanic rocks in South China (modified from Zhou *et al.* 2006); (b) simplified geological map of the Jiuhuashan–Qingyang complex.

(Shangxi Group, 50 km away) and (c) the basement beneath the Yangtze foldbelt is Proterozoic in age. However, no Proterozoic basement has previously been identified in the Yangtze foldbelt. Therefore, the age spectra of inherited zircon grains within the granitoids in this foldbelt have become a subject of interest.

The Jiuhuashan–Qingyang complex is located within the Yangzte foldbelt. Early geological and petrological investigations of the complex (e.g. Wang, Liu & Peng, 1965) revealed that the complex comprises a main body (the Qingyang granite) consisting of granodiorite and monzogranite, and a central body consisting mainly of alkali-feldspar granite (the Jiuhuashan granite). Geochronological investigations using $^{40}Ar$–$^{39}Ar$ and Sr–Nd isotopic techniques (Chen, Zhou & Foland, 1985; Chen, Foland & Zhou, 1985; Chen *et al.* 1993) indicated that the Qingyang body was formed at 137.6 ± 1.4 Ma (Rb–Sr isochron method) and the Jiuhuashan body was formed at 122.7 ± 1.2 Ma ($^{40}Ar$–$^{39}Ar$ method). However, the crystallization age of individual rock-types remains unclear.

Based on a new petrographical investigation, we carried out major and trace element analyses of representative granodiorite, monzogranite and alkali-feldspar granite, LA-ICPMS zircon U–Pb dating and CHIME dating in order to understand better the crystallization and the genetic relationship of different phases of the complex, while further constraining the characteristics of the magma source and tectonic setting by integration of regional data on Late Mesozoic granites in SE China.

## 2. General geology

The Jiuhuashan–Qingyang complex is located in South Anhui, and crops out over an area of approximately 750 km$^2$. The complex intruded into the late Precambrian to Early Palaeozoic sandstones, shales and limestones. The first stage intrusion was named the Qingyang body, which in turn was intruded by the second stage central granite named the Jiuhuashan body. Finally, a series of porphyritic syenite dykes were emplaced mostly into the Qingyang body. A detailed petrographical study and geological mapping completed by Wang, Liu & Peng (1965) have been simplified as Figure 1b and indicate that the Jiuhuashan–Qingyang complex was formed in three stages.

The main Qingyang body can be further divided into two phases: a marginal granodiorite with fine to medium granitic texture and an inner medium-grained to porphyritic monzogranite. A swarm of quenched enclaves with typical chilled margins and back-veins infiltrated from host magma (Fig. 2) have been found in the northeast part of the Qingyang body. These fine-grained, igneous-textured enclaves are igneous in origin, and are usually interpreted as globules of a separate magma, mingled with the volumetrically dominant host magma.

Modal mineral compositions of the complex are listed in Table 1. All granodiorite samples are medium-grained and lack foliation. Sample JH03 collected near the contact with monzogranite is more felsic than samples JH10 and JH11 away from the boundary. Hornblende is present in the granodioritic rocks but is sparse in the monzogranite. Monzogranite samples JH01 and JH02 were collected from an active quarry and are characterized by phenocrysts (5–10 mm) of pink-coloured microperthite.

In the second emplacement stage, the Jiuhuashan body, which crops out over about 100 km$^2$, was emplaced as a N–S elongate body that cuts across the boundary between the granodiorite and monzogranite components of the first stage. The Jiuhuashan body is generally equigranular, of medium to coarse grain size, and is dominated by microperthite and quartz, with minor albite, biotite and accessory zircon, apatite, allanite, magnetite, thorite and fergusonite (Table 1).

https://doi.org/10.1017/S0016756809990367 Published online by Cambridge University Press

Table 1. The mineral constitutents of Jiuhuashan–Qingyang complex

| | First stage (Qingyang body) | | Second stage (Jiuhuashan body) | Third stage | |
|---|---|---|---|---|---|
| Lithology | Granodiorite (Marginal phase) | Monzogranite (Inner phase) | Alkali-feldspar granite | Albite granite (Metasomatized) | Porphyritic syenite |
| Microperthite | 26 | 35 | 56 | 8 | 89.6 |
| Plagioclase | 46 (An% = 34–41) | 35 (An% = 31–37) | 2 (An% = 4–9) | 61 (An% = 4–9) | 3.5 |
| Quartz | 22 | 21 | 36 | 25 | 5 |
| Amphibole | 4 | | | | |
| Biotite | 5 | 8 | 2 | 6 | 2 |
| Muscovite | | | 1 | | |
| Accessory minerals | Apatite, magnetite, titanite, allanite and zircon | | Zircon, apatite, allanite, magnetite, thorite and fergusonite | | Apatite, magnetite and zircon |

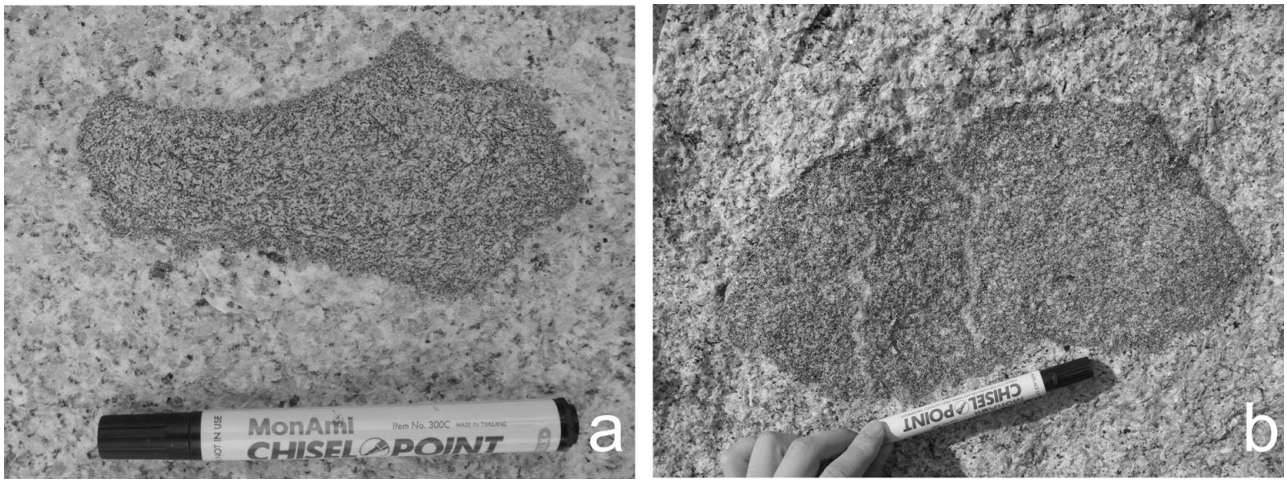


Figure 2. Quenched enclaves found in the Qingyang body: (a) typical chilled margin; (b) back-vein. The ink pen is 14.5 cm long.

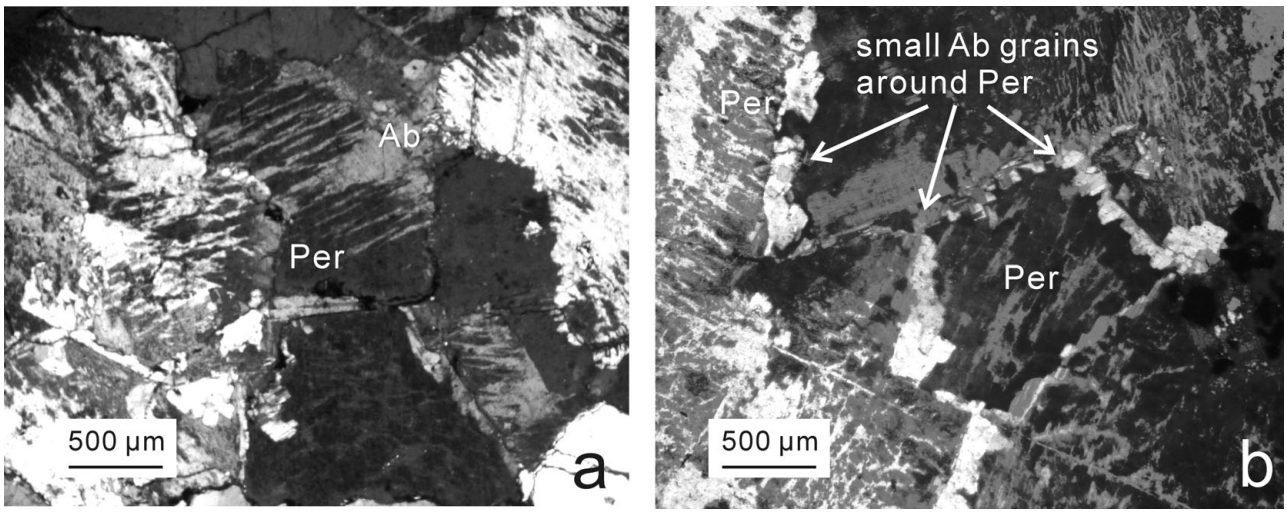


Figure 3. Photomicrographs of metasomatized alkali-feldspar granite in cross-polarized transmitted light. Ab – albite; Per – microperthite.

Five samples of alkali-feldspar granite (JH05, JH06, JH07, JH08 and JH09) were collected from the Jiuhuashan body during this study.

The third and final stage of magmatism is represented by the porphyritic syenite dykes, most of which have a graphic texture. The dykes range from several metres up to hundreds of metres in width and extend to kilometres in length, and most have a N–S strike. They are concentrated in the northern part of the complex and they intrude all the other phases of the complex. The Jiuhuashan granite may have been metasomatized following the emplacement of these dykes, resulting in the formation of albite granite. Microstructure investigations show that albite veins are commonly developed on primary K-feldspar, and therefore formed microperthite (Fig. 3a). Sometimes the fine-grained albites occur as rims around microperthite, implying that they are of metasomatic origin (Fig. 3b). In some samples, almost all of the microperthite has been replaced by albite (Wang, Liu & Peng, 1965).

https://doi.org/10.1017/S0016756809990367 Published online by Cambridge University Press

Table 2. XRF analyses of granitoids from the Jiuhuashan–Qingyang complex

| | Qingyang body | | | | Jiuhuashan body | | | |
|---|---|---|---|---|---|---|---|---|
| | Granodiorite (marginal phase) | | | Monzogranite (inner phase) | Alkali-feldspar granite | | | |
| Sample no. | JH03 | JH10 | JH11 | JH01 | JH05 | JH06 | JH07 | JH08 |
| $SiO_2$ | 68.45 | 65.64 | 67.42 | 72.13 | 74.32 | 74.71 | 75.54 | 75.15 |
| $TiO_2$ | 0.32 | 0.55 | 0.49 | 0.23 | 0.06 | 0.05 | 0.06 | 0.08 |
| $Al_2O_3$ | 15.00 | 15.13 | 14.70 | 13.43 | 12.37 | 12.24 | 11.95 | 12.35 |
| $Fe_2O_3$ | 2.73 | 4.33 | 3.61 | 1.90 | 1.24 | 0.95 | 0.82 | 1.25 |
| MnO | 0.05 | 0.08 | 0.07 | 0.07 | 0.07 | 0.09 | 0.07 | 0.04 |
| MgO | 0.77 | 1.54 | 1.26 | 0.39 | 0.00 | 0.00 | 0.01 | 0.01 |
| CaO | 2.44 | 3.41 | 3.18 | 1.37 | 0.34 | 0.06 | 0.34 | 0.32 |
| $Na_2O$ | 4.36 | 3.75 | 3.82 | 3.77 | 4.28 | 4.20 | 4.05 | 4.31 |
| $K_2O$ | 3.35 | 3.34 | 3.35 | 4.29 | 4.26 | 4.22 | 4.27 | 4.56 |
| $P_2O_5$ | 0.11 | 0.19 | 0.16 | 0.06 | 0.00 | 0.00 | 0.00 | 0.01 |
| Total | 97.59 | 97.95 | 98.06 | 97.63 | 96.94 | 96.53 | 97.11 | 98.08 |

The development of discrete albite suggests that the Jiuhuashan body underwent some metasomatic alteration after solidification.

## 3. Analytical methods

After petrographical examination, fresh rock samples were selected for zircon separation, major and trace element analyses. Major elements were determined on fused glass discs by a SHIMADZU XRF 1800 sequential X-ray fluorescence spectrometer (XRF) at the Center for Chronological Research, Nagoya University. The glass discs were prepared by fusion of a mixture with 0.7 g sample powder and 6.0 g lithium borate. Trace elements were analysed in the State Key Laboratory of Mineral Deposits Research, Nanjing University, China, by the solution method using a Finnigan Element II Inductively Coupled Plasma Mass Spectrometer (ICP-MS) (details of the analytical method are given by Jiang, Yu & Lu, 2004). Comparative analysis of fused glass samples was conducted in the same laboratory on an Agilent 7500a ICP-MS equipped with a New Wave Research 213 nm laser ablation system. Overall procedures used were similar to Norman *et al.* (1996, 1998), except for the laser system. The analyses were calibrated against the spiked silicate glass reference STD610; KL2-G was analysed to monitor accuracy.

Zircons were separated from four representative samples through standard density and magnetic separation techniques. Random zircon grains were hand-picked under a binocular microscope and mounted in a 1.4 cm diameter epoxy disc, and polished to expose the central parts of the crystals. In order to characterize the internal structures of the zircons and to choose appropriate target sites for U–Pb dating, backscattered electron (BSE) images were obtained using a JEOL JXA-8800 microprobe at Nanjing University with a 15 kV accelerating voltage and 20 nA beam current.

Zircon U–Pb analyses were carried out by LA-ICPMS on the Agilent 7500a at Nanjing University. Analyses were carried out with a beam diameter of 30–40 μm, 5 Hz repetition rate, and energy of 10–20 $J \cdot cm^{-2}$. Data acquisition for each analysis took 120 s (40 s on background, 80 s on signal). Raw count rates for $^{206}Pb$, $^{207}Pb$, $^{208}Pb$, $^{232}Th$ and $^{238}U$ were collected for age determination. Mass discrimination of the mass spectrometer and residual elemental fractionation were corrected by calibration against a homogeneous standard zircon, GEMOC/GJ-1 (601 Ma). Samples were analysed in 'runs' of about 18 analyses, which include 10–12 unknowns, bracketed beginning and end by two to four analyses of the standard. The 'unknowns' include two analyses of the well-characterized Mud Tank zircon (735 Ma), which were analysed frequently to monitor the reproducibility and the stability of instrument. Details of instrument settings and analytical procedures followed Jackson *et al.* (2004).

Raw ICP-MS data were processed using the program GLITTER (van Achterbergh *et al.* 2001). Common Pb contents were evaluated using the method described by Andersen (2002). Age calculations and concordia plots were made using Isoplot (ver. 2.49) (Ludwig, 2001). The concentrations of U and Th in each analytical spot were derived by comparison of background-corrected count rates with mean count rates on the GJ-1 standard, which has well-defined concentrations of these two elements.

Zircon and monazite in JH08 alkali-feldspar granite were dated by the CHIME method (Chemical Th–U–total Pb Isochron Method: Suzuki & Adachi, 1991) using a JCXA-733 EPMA with 4 WDSs at the Center for Chronological Research, Nagoya University. Details of experimental techniques for CHIME dating were described in Suzuki & Kato (2008).

## 4. Results

### 4.a. Major element geochemistry

Eight representative fresh samples were selected for major element analysis and the results are listed in Table 2. Samples from the marginal phase (JH03, JH10 and JH11) of the Qingyang body are granodiorite with $SiO_2$ ranging from 65.6 % to 68.5 % and $K_2O+Na_2O$ from 7.09 % to 7.72 %. As noted above, JH03 is located close to the boundary between the marginal and inner phases, and JH10 furthest away from the boundary.

https://doi.org/10.1017/S0016756809990367 Published online by Cambridge University Press

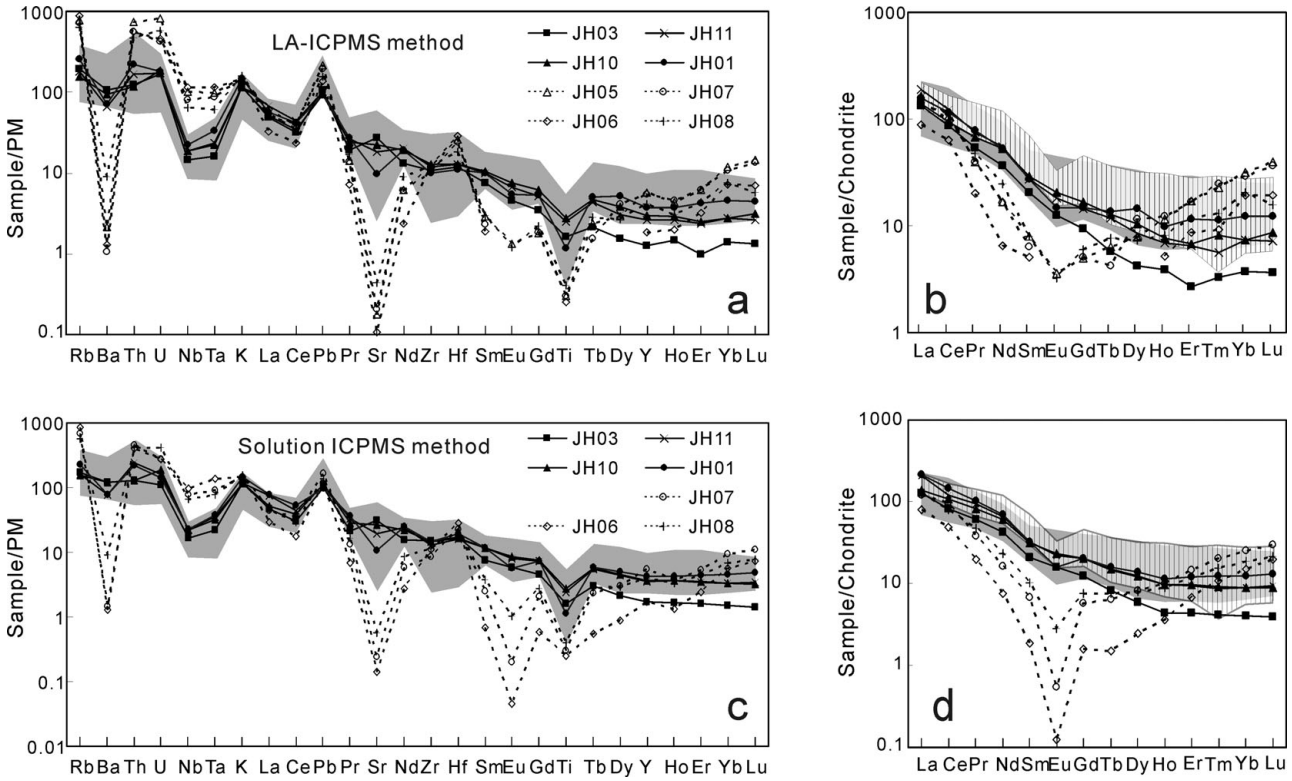


Figure 4. Primitive mantle-normalized trace element diagram (a, c) and chondrite-normalized REE patterns (b, d) of the Jiuhuashan–Qingyang complex. The chondrite values and primitive mantle values are after Anders & Grevesse (1989) and McDonough & Sun (1995), respectively. Grey area: Late Yanshanian calc-alkaline granites in the coastal area of SE China (25 analyses from Li & Zhou, 2000; Xie *et al.* 2003; Geng *et al*. 2006). Hatched area: Late Yanshanian granites in the NE Yangtze Block (17 analyses from Yuan *et al.* 2003).

Increase of $SiO_2$ contents towards the centre is accompanied by decreases in FeO, MgO and CaO and is consistent with the marginal phase having solidified inwards with a significant differentiation of the magma. Compared with even the most evolved marginal phase sample (JH03), sample JH01 of the Qingyang body inner phase has higher $SiO_2$ (72.1 %) and $K_2O+Na_2O$ (8.06 %) contents combined with lower $Fe_2O_3$, MgO and CaO contents. Samples from the Jiuhuashan body have higher $SiO_2$ (74.3–75.5 %) and $K_2O+Na_2O$ (8.32–8.87 %) abundances and are alkali-feldspar granites.

The molar $Al_2O_3/(CaO+Na_2O+K_2O)$ ratios are 0.94–0.98 for the marginal granodiorites, 1.01 for the inner monzogranite and 0.98–1.07 for the central alkali-feldspar granites. The molar $(K_2O+Na_2O)/Al_2O_3$ ratios are 0.64–0.81 for the marginal granodiorites, and 0.81 for the inner monzogranite. Alkali-feldspar granites of the Jiuhuashan body have molar $(K_2O+Na_2O)/Al_2O_3$ ratios higher than 0.94.

#### 4.b. Trace element geochemistry

The trace element analyses for representative samples are presented in Table 3. ICP-MS results of both laser ablation on fused glass samples (LA) and solution samples (S) are reasonably consistent (see Fig. 4). The Eu concentrations in alkali-feldspar granites of the Jiuhuashan body are close to or below the detection limit of the LA-ICPMS analyses. Overall, the analytical data from solution samples are more precise with lower detection limits, but results obtained by both methods can be used for the following discussion.

The Qingyang granodiorite and monzogranite samples have Rb/Sr ratios < 1, with Rb between 93–154 ppm and Sr between 189–617 ppm. The Zr/Hf ratios vary little (27.7–36.9). The Jiuhuashan granites have much higher Rb/Sr ratios (> 30), with very high Rb (> 343 ppm) and very low Sr (< 11.2 ppm) contents. The Zr/Hf ratios of Jiuhuashan granites are consistently lower (13.8–24.4) than those of the Qingyang granodiorite and monzogranite. The Ce/Pb and Nb/U ratios of Qingyang granodiorite and monzogranite are also different from those of the Jiuhuashan granites.

On the primitive mantle normalization spider diagram (Fig. 4a, c), the Qingyang granodiorite and monzogranite display similar patterns that are characterized by consistent enrichment toward the larger ionic elements. Jiuhuashan alkali-feldspar granites are similar to each other, and are characterized by enrichment in Rb, Th, U, Nb, Ta and Hf, and depletion in Ba, Sr, Nd, Sm, Eu, Gd and Ti, which are obviously different from patterns for Qingyang granodiorite and monzogranite. The chondrite-normalized REE patterns are shown on the right side in Figure 4b and d. The patterns also show significant differences between the Qingyang and Jiuhuashan granitic samples. The Qingyang granodiorite and monzogranite samples

https://doi.org/10.1017/S0016756809990367 Published online by Cambridge University Press

Table 3. Trace element compositions analysed by LA-ICPMS method (LA) and solution method (S)

| Sample no. | JH03 | | JH10 | | JH11 | | JH01 | | JH05 | JH06 | | JH07 | | JH08 | |
|---|---|---|---|---|---|---|---|---|---|---|---|---|---|---|---|
| Method | LA | S | LA | S | LA | S | LA | S | LA | LA | S | LA | S | LA | S |
| Rb | 117 | 102 | 94 | 93 | 107 | 95 | 154 | 137 | 464 | 535 | 505 | 437 | 405 | 378 | 343 |
| Ba | 699 | 810 | 622 | 798 | 432 | 516 | 464 | 514 | 14 | 8 | 8 | 7 | 10 | 58 | 60 |
| Th | 9.85 | 10.09 | 9.37 | 10.26 | 13.26 | 19.41 | 17.43 | 17.62 | 59.22 | 44.52 | 31.39 | 44.41 | 36.03 | 37.73 | 33.13 |
| U | 3.42 | 2.23 | 3.77 | 3.81 | 3.51 | 3.31 | 3.69 | 2.91 | 16.55 | 9.34 | 5.54 | 8.67 | 5.60 | 11.57 | 8.35 |
| Nb | 9.43 | 10.74 | 12.17 | 14.61 | 12.25 | 14.97 | 14.56 | 15.14 | 65.41 | 74.78 | 62.82 | 52.64 | 50.63 | 41.84 | 43.65 |
| Ta | 0.59 | 0.82 | 0.83 | 1.20 | 0.87 | 1.31 | 1.23 | 1.38 | 3.60 | 4.18 | 5.08 | 3.21 | 3.39 | 2.22 | 2.87 |
| La | 31.34 | 30.15 | 32.79 | 33.04 | 44.07 | 49.43 | 36.83 | 50.71 | 38.16 | 20.83 | 18.85 | 31.02 | 28.22 | 34.99 | 29.68 |
| Ce | 52.23 | 50.37 | 57.10 | 65.72 | 73.46 | 72.78 | 68.97 | 88.21 | 64.79 | 38.71 | 29.64 | 67.63 | 59.49 | 59.00 | 48.79 |
| Pb | 15.69 | 15.12 | 14.01 | 17.11 | 15.27 | 16.44 | 13.83 | 14.75 | 32.15 | 20.63 | 17.51 | 29.01 | 24.98 | 23.12 | 20.48 |
| Pr | 4.79 | 5.49 | 6.05 | 7.29 | 6.67 | 8.38 | 6.92 | 9.26 | 3.56 | 1.79 | 1.76 | 3.52 | 3.41 | 4.27 | 4.24 |
| Sr | 544 | 617 | 436 | 529 | 362 | 385 | 189 | 209 | 3.46 | 2.11 | 2.81 | 4.00 | 4.88 | 8.65 | 11.22 |
| Nd | 16.37 | 19.51 | 24.05 | 27.33 | 24.84 | 30.15 | 24.05 | 31.43 | 7.63 | 2.92 | 3.43 | 7.40 | 7.37 | 11.09 | 10.62 |
| Zr | 113 | 160 | 134 | 153 | 122 | 136 | 104 | 152 | 124 | 126 | 117 | 107 | 90 | 125 | 118 |
| Hf | 3.33 | 4.91 | 3.64 | 4.72 | 3.60 | 4.51 | 3.12 | 5.50 | 7.28 | 8.00 | 7.96 | 6.75 | 6.50 | 5.14 | 6.23 |
| Sm | 3.05 | 3.10 | 4.26 | 4.70 | 4.03 | 4.74 | 4.01 | 4.73 | 1.18 | 0.75 | 0.27 | 0.93 | 1.01 | 1.19 | 1.52 |
| Eu | 0.70 | 0.89 | 1.16 | 1.32 | 1.01 | 1.24 | 0.83 | 0.88 | 0.20 | b.d. | 0.01 | b.d. | 0.03 | 0.18 | 0.16 |
| Gd | 1.84 | 2.46 | 3.30 | 4.06 | 2.82 | 4.02 | 2.89 | 4.01 | 0.98 | b.d. | 0.32 | 0.99 | 1.13 | 1.19 | 1.50 |
| Tb | 0.21 | 0.30 | 0.46 | 0.55 | 0.43 | 0.54 | 0.49 | 0.58 | 0.23 | b.d. | 0.05 | 0.15 | 0.23 | 0.28 | 0.28 |
| Dy | 1.03 | 1.45 | 2.56 | 3.04 | 2.05 | 2.93 | 3.48 | 3.34 | 1.91 | b.d. | 0.60 | 2.78 | 2.01 | 1.79 | 1.97 |
| Y | 5.42 | 7.25 | 12.56 | 15.56 | 11.22 | 15.21 | 16.01 | 18.31 | 24.62 | 7.74 | 7.26 | 23.33 | 23.73 | 17.34 | 17.44 |
| Ho | 0.22 | 0.25 | 0.43 | 0.54 | 0.38 | 0.54 | 0.55 | 0.64 | 0.65 | 0.29 | 0.20 | 0.68 | 0.56 | 0.45 | 0.50 |
| Er | 0.42 | 0.70 | 1.07 | 1.54 | 1.03 | 1.49 | 1.85 | 1.90 | 2.69 | 1.38 | 1.07 | 2.66 | 2.35 | 1.89 | 1.91 |
| Tm | 0.08 | 0.10 | 0.20 | 0.22 | 0.14 | 0.21 | 0.27 | 0.30 | 0.55 | 0.22 | 0.26 | 0.60 | 0.50 | 0.31 | 0.38 |
| Yb | 0.61 | 0.67 | 1.20 | 1.45 | 1.20 | 1.45 | 2.01 | 2.01 | 5.19 | 3.16 | 2.48 | 4.75 | 4.10 | 3.31 | 3.03 |
| Lu | 0.09 | 0.10 | 0.21 | 0.22 | 0.18 | 0.23 | 0.30 | 0.32 | 0.97 | 0.47 | 0.49 | 0.90 | 0.73 | 0.38 | 0.53 |
| Rb/Sr | 0.21 | 0.16 | 0.21 | 0.18 | 0.29 | 0.25 | 0.81 | 0.66 | 134.12 | 254.35 | 179.75 | 109.42 | 83.06 | 43.70 | 30.56 |
| Zr/Hf | 33.88 | 32.61 | 36.85 | 32.41 | 34.04 | 30.10 | 33.47 | 27.69 | 17.04 | 15.71 | 14.69 | 15.91 | 13.81 | 24.41 | 19.01 |
| Ce/Pb | 3.33 | 3.33 | 4.08 | 3.84 | 4.81 | 4.43 | 4.99 | 5.98 | 2.02 | 1.88 | 1.69 | 2.33 | 2.38 | 2.55 | 2.38 |
| Nb/U | 2.76 | 4.82 | 3.23 | 3.83 | 3.49 | 4.53 | 3.94 | 5.20 | 3.95 | 8.01 | 11.33 | 6.07 | 9.04 | 3.62 | 5.23 |
| $La/Yb_N$ | 35.57 | 31.31 | 19.00 | 15.74 | 25.43 | 23.68 | 12.69 | 17.48 | 5.09 | 4.56 | 5.27 | 4.52 | 4.77 | 7.33 | 6.78 |

b.d.—below detection limit.

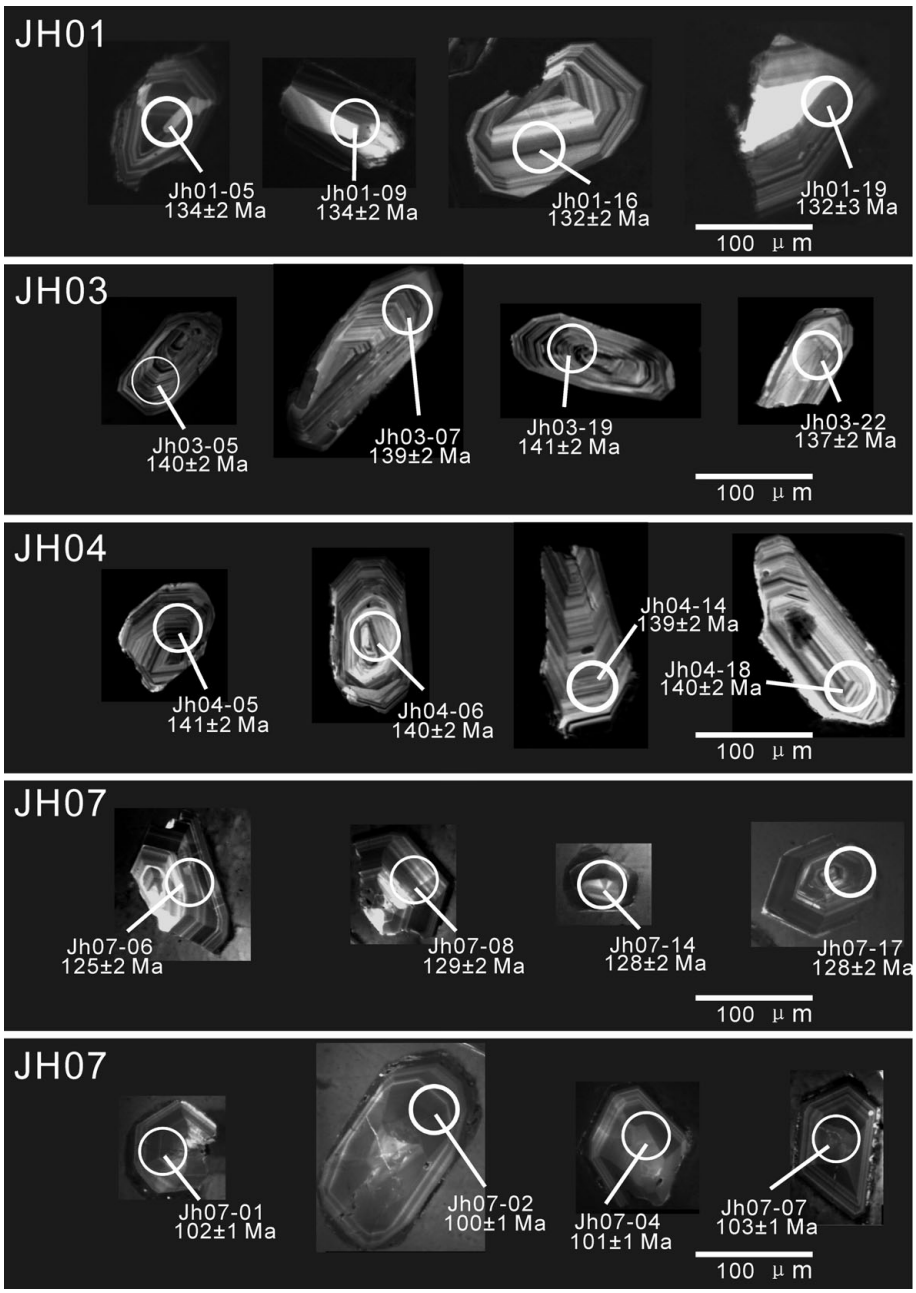


Figure 5. Backscattered electron images of representative zircons.

show consistent enrichment in La with flat heavy rare earth element patterns, while Jiuhuashan alkali-feldspar granites show a V-shaped pattern with a strong Eu negative anomaly. The $(La/Yb)_N$ ratios of the Jiuhuashan alkali-feldspar granites (4.5–7.3) are distinctly lower than those (12.7–35.6) of the Qingyang granodiorite and monzogranite.

Precise trace element (including large ion lithophile element) analysis for the granites in the Yangzte fold belt, NE Yangtze Block, has not been reported. The available rare earth element data for the other granites in this region are incorporated in Figure 4b and d. Apparently, the chondrite-normalized REE patterns of the Qingyang granodiorite and monzogranite are similar to those of other granites in the same region, while the Jiuhuashan granites show a distinct Eu negative anomaly. The trace element data from contemporary calc-alkaline granites in the coastal area of SE China are also collected and displayed in Figure 4 for comparison, and their petrogenetic implications will be discussed below.

#### 4.c. Zircon U–Pb dating

Except for a few inherited zircons (age data in Table A1, available online as supplementary material at http://www.cambridge.org/journals/geo; see discussion below), zircon crystals from the Qingyang granodiorite and monzogranite are euhedral with oscillatory zoning. Zircons from the Jiuhuashan alkali-feldspar granites are also euhedral and oscillatory zoned but many are sector zoned. Backscattered electron images (BSE) of representative zircon grains

https://doi.org/10.1017/S0016756809990367 Published online by Cambridge University Press

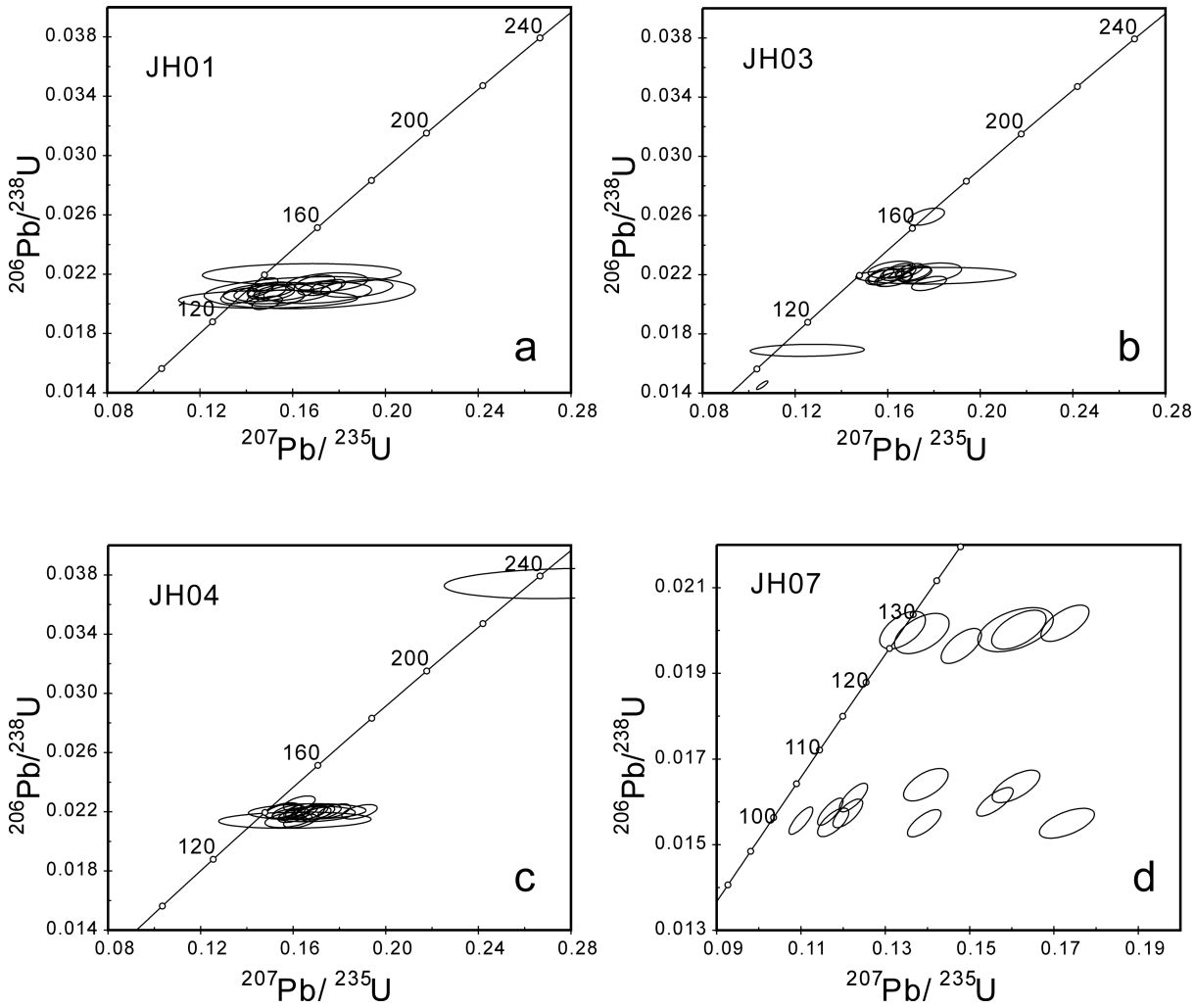


Figure 6. Zircon U–Pb concordia diagram for four samples from the Jiuhuashan–Qingyang complex.

are shown in Figure 5. Because of errors in counting statistics during the analysis, $^{207}Pb/^{206}Pb$ ages are more precise for older (> 1 Ga) zircons, while $^{206}Pb/^{238}U$ ages are more precise for younger zircons (Griffin *et al.* 2004). Therefore, we use the $^{207}Pb/^{206}Pb$ ages for older (> 1 Ga) zircons and $^{206}Pb/^{238}U$ ages for younger zircons (Table A1) in the following discussion. Concordia plots and weighted averages (Figs 6, 7) were constructed using Isoplot 2.49 (Ludwig, 2001).

Most of the zircons separated from two rock samples (JH03 and JH04) of the marginal phase are concordant (Fig. 6b, c); main populations of the two samples both give ages of about 140 Ma, but two grains (JH03–01 and JH04–12, Table A1), interpreted as inherited, give ages of 165 Ma and 237 Ma, respectively. In addition, two grains from sample JH03 give younger $^{206}Pb/^{238}U$ ages of 93 Ma and 108 Ma, respectively, which may represent the age of metasomatism (see discussion below). The main populations for the two rock samples yield weighted mean $^{206}Pb/^{238}U$ ages of $140.0 \pm 1.1$ Ma (n = 14, MSWD = 0.64) and $139.7 \pm 0.9$ Ma (n = 19, MSWD = 0.77), respectively. Except for one zircon grain (JH01–10, Table A1) which is Archaean (2557 Ma), all other zircons separated from the inner phase of the Qingyang body plot on or near concordia (Fig. 6a). The weighted mean age of 19 zircons is $133.2 \pm 1.3$ Ma (MSWD = 1.5, Fig. 7), significantly younger than the marginal phase.

Zircons separated from a single rock sample (JH07) of the Jiuhuashan body show two distinct age groups on the concordia plot (Fig. 6d), but most are discordant. The weighted mean $^{206}Pb/^{238}U$ age of one group is $127.5 \pm 1.6$ Ma (MSWD = 0.47), while that of the other group is $100.8 \pm 1.3$ Ma (MSWD = 2.8, Fig. 7).

#### 4.d. CHIME monazite and zircon dating

Monazite and zircon in JH08 alkali-feldspar granite were dated by the CHIME method (for analytical data see Appendix Table A2, available online at http://www.cambridge.org/journals/geo). Monazites form subhedral grains 0.1–0.2 mm in length, and occur mostly in quartz or along grain boundaries between main constituents. A total of 63 spots were analysed. The $ThO_2$ content ranges from 1.26 to 11.9 wt %, the $UO_2$ content from 0.02 to 0.47 wt % and the $Y_2O_3$ content from 0.10 to 0.83 wt %. Many analyses show high

https://doi.org/10.1017/S0016756809990367 Published online by Cambridge University Press

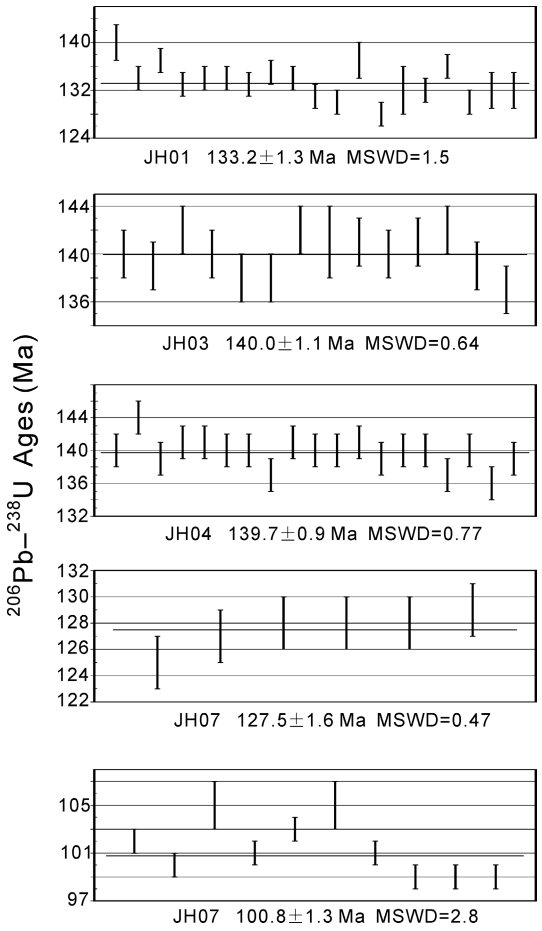


Figure 7. Weighted average $^{206}$Pb–$^{238}$U ages for four samples from the Jiuhuashan-Qingyang complex.

concentration of K, and the (Ca+Si)/(Th+U+Pb+S) ratio deviated from unity; these are used as criteria for discordance (Suzuki & Kato, 2008). Possibly concordant analyses, therefore, were screened by the criteria $K_2O < 0.015$ wt % (close to the detection limits at 2 sigma) and $0.95 < (Ca+Si)/(Th+U+Pb+S) < 1.05$. The screened monazites form two different trends on the diagram: data points on the upper trend (solid circles, > 110 Ma in apparent age) define an isochron of $127.6 \pm 5.3$ Ma, and those on the lower trend (open squares) yield an isochron of $96.1 \pm 6.3$ Ma (Fig. 8a). The spots showing younger ages tend to be located on marginal parts of the analysed grain. Zircon analyses were screened with chemical criteria: $CaO < 0.015$ and $K_2O < 0.015$ (Suzuki & Kato, 2008). The screened 22 analyses (of 50) were classified into two groups. Isochron analyses with apparent ages older than 110 Ma give $129.1 \pm 10.1$ Ma and the rest give $90.8 \pm 9.9$ Ma (Fig. 8b). Although showing a much larger possible age range, the CHIME monazite and zircon ages agree well with the LA-ICPMS zircon ages of $127.5 \pm 1.6$ and $100.8 \pm 1.3$ Ma.

## 5. Discussion

The above dating results clearly show that the marginal granodiorite of the Qingyang body was crystallized at 140 Ma, and the inner monzogranite of the Qingyang body was crystallized at 133 Ma. Inherited zircons in granodiorite and monzogranite suggest involvement of both Mesozoic (237 Ma and 165 Ma) and Neoarchaean (2557 Ma) materials in magmas of the Qingyang body. The implications of dating

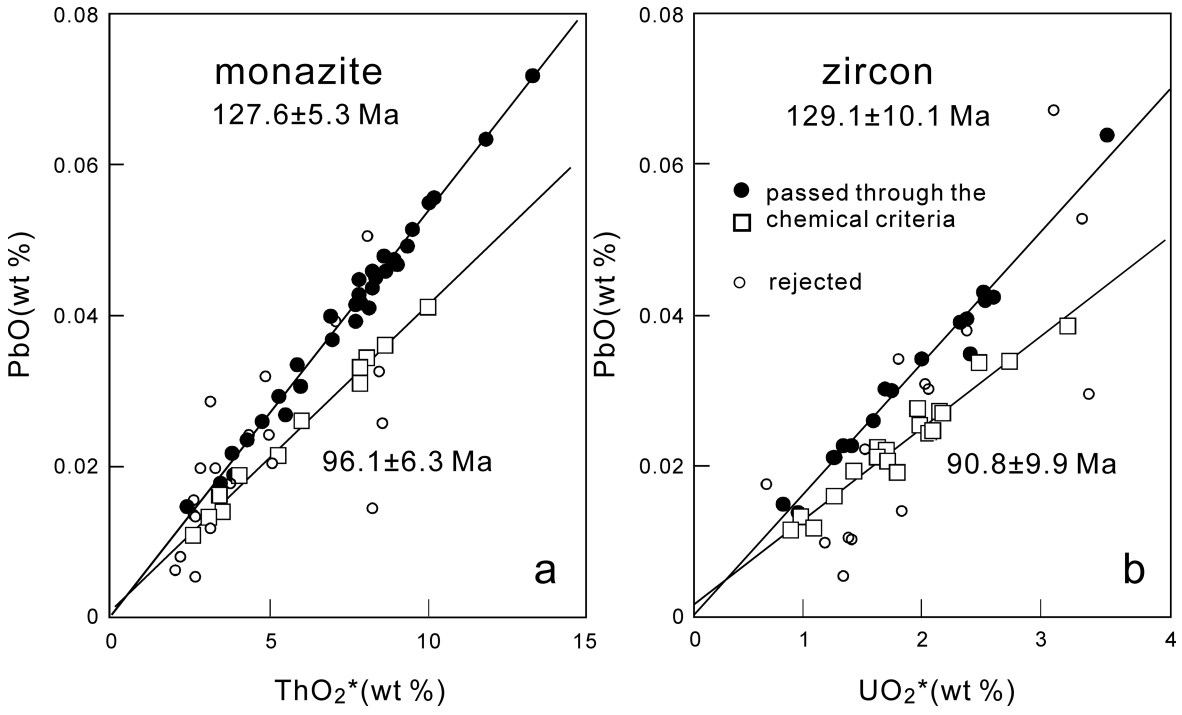


Figure 8. CHIME plots of (a) monazite and (b) zircon from JH08 alkali-feldspar granite in the Jiuhuashan body. $ThO_2^*$ shows the sum of the measured $ThO_2$ and $ThO_2$ equivalent to the measured $UO_2$, and $UO_2^*$ shows the sum of the measured $UO_2$ and $UO_2$ equivalent to the measured $ThO_2$.

https://doi.org/10.1017/S0016756809990367 Published online by Cambridge University Press

results for the Jiuhuashan alkali-feldspar granite body need to be further discussed, including petrographical input.

Petrographical observations show that Jiuhuashan alkali-feldspar granite experienced a metasomatic event that developed albite veins on K-feldspar and formed the microperthite. The replacement starts from the mineral margin, and sometimes almost all microperthites are replaced by albite, therefore the metasomatic agent should be sodium-rich. Although zircons are known to be stable in various geological environments and are suitable for U–Th–Pb age dating, several studies showed the disruption of the isotopic system at temperatures below 900 °C in the presence of fluids (e.g. Rizvanova *et al.* 2000; Cherniak & Watson, 2000; Geisler *et al.* 2003*a*,*b*; Martin *et al.* 2006). Metamict (radiation-damaged) grains or portions of a single grain can easily re-crystallize under hydrothermal conditions (Geisler *et al.* 2001); hydrothermal zircons can be formed during sodic metasomatism (albitization) (Pelleter *et al.* 2007) and may be used for hydrothermal event dating (Geisler *et al.* 2003*b*; Pelleter *et al.* 2007). However, hydrothermal zircon is an 'imprecise term' that refers to all zircons crystallized from, or altered by, an aqueous fluid (Hoskin, 2005) and is difficult to distinguish from magmatic zircon.

The present dating disclosed two different ages for crystallization and metasomatism for the Jiuhuashan alkali-feldspar granites. Because of the metasomatism, some of the zircons were recrystallized, especially those at the rim of microperthite and showing disconcordance on the concordia plot (Fig. 6). We believe that the age of 127 Ma represents the crystallization age, and the age of 100 Ma may date the metasomatic event. This explanation is supported by published $^{40}Ar$–$^{39}Ar$ dates that gave an age of 122.7 ± 1.2 Ma for the Jiuhuashan alkali-feldspar granite (Chen, Zhou & Foland, 1985; Chen, Foland & Zhou, 1985; Chen *et al.* 1993). The two age groups of zircons have distinct differences in U and Th abundance, that is, the older (magmatic) zircons have low U (< 1558 ppm) and Th (< 2860 ppm), and U+Th < 4418 ppm, while the younger (hydrothermal) zircons have high U (> 3197 ppm) and Th (> 4321 ppm), and U+Th > 7518 ppm. The metasomatic event also partly reset the zircon ages in the Qingyang body, that is, the zircons with younger resetting ages (*c.* 100 Ma) have also been identified in the Qingyang granite (JH03–02 and JH03–06 in Table A1 and Fig. 6). Therefore, the *c.* 100 Ma ages of zircon and monazite likely represent the time of the metasomatic alteration in the Jiuhuashan complex.

Chen, Foland & Zhou (1985) and Chen *et al.* (1993) analysed the Sr–Nd and oxygen isotopes of the Jiuhuashan complex. Both Qingyang granodiorite and Jiuhuashan granite have similar initial $^{87}Sr/^{86}Sr$ and $^{143}Nd/^{144}Nd$ ratios of about 0.7085 and 0.51220, respectively. Overall, whole-rock $\delta^{18}O$ values range from 7.0 to 9.9 ‰, and therefore minor isotopic heterogeneities are apparent. The high Sr initial ratios, low Nd initial ratios and high $\delta^{18}O$ values indicate the dominance of old crust in the formation of these granitoid magmas. Chen, Foland & Zhou (1985) and Chen *et al.* (1993) argued that the magmas were produced by crustal anatexis and that no mantle melts were involved directly in the production of the granitoids. They further postulated Proterozoic ages for source rocks (Proterozoic Shangxi Group) on the basis of the Nd model ages of 1000 to 1170 Ma. However, field geological investigations show there is a swarm of mafic enclaves in the Qingyang body. The presence of typical chilled margins on some enclaves is evidence of a syn-plutonic intrusion of basaltic magma, and therefore the previous interpretation for Sr and Nd isotopic compositions should be revisited. Firstly, if the isotopic characteristics of the magmas are very similar to those of the Proterozoic metamorphic rocks (Shangxi Group), then they should have older Nd model ages (> 1400 Ma) (Chen & Jahn, 1998). Secondly, the contemporary Yaocun granite (132 Ma) in the same region was generated apparently with juvenile input, which should be mantle-derived magma; the dark enclaves were formed by incomplete mixing of intermediate–basic magma with granitic magma (Ling, Zhai & Zhang, 1990). Thirdly, nearby contemporary mafic rocks (e.g. gabbro in 30 km north with an age of 137 Ma: Wu *et al.* 1996) show enriched Sr–Nd isotopic characteristics, with initial $^{87}Sr/^{86}Sr$ ranging from 0.7056 to 0.7071 and $^{143}Nd/^{144}Nd$ ratios of about 0.51214 to 0.51234, indicating an origin from enriched lithospheric mantle (Yan, Chen & Xu, 2008). In fact, normal geothermal gradients are seldom sufficient to provide the necessary heat for partial melting of the crust. Crustal doubling, by thrusting or homogeneous thickening, likewise fails to provide sufficient heat. The extra heat required might be provided through mantle upwelling and crustal thinning, and possibly through the intra- and underplating of mafic magmas (Clemens, 2003 and references therein). The dark, microgranular igneous-textured enclaves occurring in the Qingyang body may represent globules of quenched, more mafic magma mingled with the host granitic magma. Therefore, although the Jiuhuashan–Qingyang complex shows S-type granite affinity, it is likely that limited mantle-derived magma was involved directly in the production of the granitoids.

The younger Nd model ages (*c.* 1000 to 1170 Ma) of the granitoid magmas could have resulted from anatexis of old crust (Nd model ages > 1800 Ma, and with Neoarchaean relics) mixed with limited juvenile material. Compared with the suggested ratios of OIB (Ce/Pb ≈ 25 ± 5; Nb/U ≈ 47 ± 10), primitive mantle (Ce/Pb ≈ 9 and Nb/U ≈ 30) and continental crust (Ce/Pb ≈ 4 and Nb/U ≈ 10) (Hofmann *et al.* 1986), the Ce/Pb and Nb/U ratios of the Qingyang granodiorite and monzogranite, and that of the Jiuhuashan alkali-feldspar granites imply that they are basically derived by crustal melting. The Ce/Pb ratio of the Qingyang granodiorite could be as high as 5.98

https://doi.org/10.1017/S0016756809990367 Published online by Cambridge University Press

(Table 3), however, which may again imply the mixing of limited juvenile material during the magma generation.

The very different trace element abundances of the Qingyang and Jiuhuashan bodies could be due to either the difference in source rock composition or the difference in degree of fractionation. The close similarity in initial Sr and Nd isotopic ratios seems to favour the second option.

As the whole-rock Sr and Eu are hosted mainly in plagioclase, and the Ba, Ti, Fe and Mg are hosted mainly in biotite, the depletion of these elements in the Jiuhuashan body may reflect the separation of plagioclase and biotite. Depletion in whole-rock Ca stabilizes monazite instead of allanite in alkali-feldspar granite of the Jiuhuashan body. Evidently, monazite behaves as a major repository of lighter rare earth elements. Alkali-feldspar granites in the Jiuhuashan body contain substantial amounts of thorite, while the mode of zircon remains unchanged. Thorite incorporates heavy rare earth elements, giving a convex-upward chondrite-normalized REE pattern with a maximum around Dy (Suzuki, Adachi & Yamamoto, 1990). The high content of Nb in alkali-feldspar granites is due to the presence of minute amounts of fergusonite. This mineral shows a strong presence of heavy rare earth elements; the Yb and Lu contents could be as high as 4 and 0.5 wt %, respectively (Suzuki, Adachi & Yamamoto, 1990). The combined effect of the plagioclase, monazite, thorite and fergsonite REE patterns accounts for the V-shaped normalized REE pattern of highly evolved Jiuhuashan alkali-feldspar granites.

The dating results coupled with the geochemical studies suggest that the Jiuhuashan–Qingyang complex formed by initial ballooning of the Qingyang body and subsequent upwelling of the mobile Jiuhuashan body, similarly to the Bergell pluton in the border of Switzerland and Italy (Pitcher, 1997). In the first stage, a large volume of magma rose as a balloon to the level of neutral buoyancy and solidified gradually, from the marginal part at *c.* 140 Ma to the inner part at *c.* 133 Ma, with magmatic differentiation. This ballooning was possibly triggered by the intrusion/underplating of basaltic magma, as indicated by numerous enclaves with chilled margins. In the second stage, because of the extensional tectonic setting (Yan *et al.* 2009), highly evolved magma of the Jiuhuashan body was pushed aside by the pre-emplaced Qingyang body, and crystallized at 127 Ma. In the third stage (*c.* 100 Ma), parts of the alkali-feldspar granite changed into albite granite because of metasomatic infiltration of Na-rich fluid that was probably liberated from crystallizing syenite dykes.

Therefore, the present study provides ages which are consistent with the previous dating results (Chen, Zhou & Foland, 1985; Chen, Foland & Zhou, 1985) obtained by different methods. This work also provides additional constraints on the genesis, source materials, emplacement mechanism and metasomatic overprint of the Jiuhuashan–Qingyang complex.

The isotopic age histogram of Mesozoic granite-volcanic rocks of SE China shows that there was about a 25 Ma magmatically inactive period during Early Jurassic times (205–180 Ma). This tectonic quiescence is regarded as the tectonic regime change from the influence of the Indosinian orogeny as part of the large-scale Tethyan tectonics to the influence of the Yanshanian orogeny genetically associated with the western Pacific tectonics (Zhou *et al.* 2006). Therefore, SE China became an active continental margin from Jurassic to Cretaceous time (Zhou & Li, 2000; Zhou *et al.* 2006), and the margin was related to the subduction of the palaeo-Pacific plate. The Late Mesozoic granitoid-volcanic rocks were the products of the NW–WNW subduction of the palaeo-Pacific plate beneath the eastern Asian continent. In detail, the Late Mesozoic magmatism in the SE China underwent three stages (Zhou *et al.* 2006): (1) intraplate magmatism including initial rift-type magmatism at the Early Yanshanian stage (Middle to Late Jurassic period), (2) continental margin arc magmatism at the early Late Yanshanian stage (Early Cretaceous), and (3) tholeiitic basalt volcanism recorded in red beds of back-arc basins at the Late Yanshanian stage (Late Cretaceous).

Although agreeing that Cretaceous magmatism in eastern China was mainly controlled by the subduction of the Pacific plate, Sun *et al.* (2007) argued that the Cretaceous geological evolution matches well with the drifting history of the Pacific plate, and proposed that the major tectonic change from extension to transpression in eastern China occurred contemporaneously with an abrupt change of $\sim 80^{\circ}$ in the drifting direction of the subducting Pacific plate, that is, the drifting direction of the Pacific plate has changed several times since 140 Ma. The first major event occurred at 125–122 Ma, when the drifting direction changed from roughly southward to northwestward.

We tend to favour the idea that granites in Yangtze foldbelt (NE Yangtze Block) were controlled by the northwestward subduction of the Pacific plate, because (1) the Yangtze foldbelt is NE-striking tectonically; (2) most of the granite bodies in this region are enlongated in a NE–SW orientation, which is consistent with the distribution of regional Late Yanshanian granites in the coastal area.

Preliminary comparisons of trace element (including large ion lithophile element) analyses for the Late Yanshanian granites in the Yangzte fold belt and in the coastal area of SE China (Fig. 4) show that their spider diagram and chondrite-normalized REE patterns are similar, except for the evolved Jiuhuashan granites. Xu *et al.* (1999) and Zhou *et al.* (2006) recognized that the extension-induced deep crustal melting and the underplating of basaltic magmas were the two main driving forces for the Yanshanian granitic magmatism in the coastal area of SE China. As discussed above, the Late Yanshanian granites in the Yangzte fold belt were produced in the same tectonic setting as the granites in the coastal area. Their Sr–Nd isotope compositions

are also similar, with initial Sr isotope ratios (0.7058–0.7104) and epsilon Nd values (−5 to −7) (Chen *et al.* 1993) for the Late Yanshanian granites in the Jiangnan zone of the Yangzte fold belt, and similar to the initial Sr isotope ratios (average 0.71012) and epsilon Nd values (average −6.97) for all of the Late Yanshanian granites in SE China (Shen, Ling & Sun, 2007). However, they were developed on different crustal basement (Fig. 1), and the granites in the NE Yangtze Block were basically derived by crustal melting with limited mixing of juvenile material during magma generation.

## 6. Conclusions

The Jiuhuashan–Qingyang complex in southern Anhui is subdivided into the main Qingyang body and the central Jiuhuashan body. Integrating petrographical, petrochemical and geochronological data, we draw the following conclusions:

(1) The Qingyang body of the complex was formed during the Cretaceous period, its marginal phase was crystallized at 140 Ma, and the inner phase was crystallized at *c.* 133 Ma. Neoarchaean restitic zircon was detected in this study, which suggests the involvement of old lower crust materials during the magmatism. In conjunction with petrographical studies, both LA-ICPMS zircon U–Pb ages and the CHIME monazite and zircon ages show that the Jiuhuashan body was crystallized at 127 Ma, and experienced metasomatism at *c.* 100 Ma.

(2) The enrichment of Rb, Th, U, Nb, Ta and Hf, depletion of Ba, Sr, Nd, Sm, Eu, Gd and Ti on the spider diagram, and the V-shaped normalized REE pattern of the Jiuhuashan alkali-feldspar granites are ascribable to the separation of plagioclase and biotite, and crystallization of thorite and fergusonite.

(3) The Jiuhuashan–Qingyang complex, together with other granites in the NE Yangtze Block, was derived by crustal anatexis but with limited mixing of juvenile material during the magma generation, which was triggered by the northwestward subduction of the Pacific plate.

**Acknowledgements.** We thank He ZY for help with zircon U–Pb dating, Dr Richard Flood, two anonymous reviewers and editor Professor David Pyle for their very helpful comments. This research was financially supported by the National Natural Science Foundation of China (grant no. 40730313), National Major Basic Research Project of China (2006CB403508) and research grant (2008-I-02) from the State Key Laboratory for Mineral Deposits Research, Nanjing University.

## References

ANDERS, E. & GREVESSE, N. 1989. Abundances of the elements: Meteoritic and solar. *Geochimica et Cosmochimica Acta* **53**, 197–214.

ANDERSEN, T. 2002. Correction of common Pb in U–Pb analyses that do not report $^{204}$Pb. *Chemical Geology* **192**, 59–79.

CHARVET, J., SHU, L., SHI, Y., GUO, L. & FAURE, M. 1996. The building of south China: collision of Yangzi and Cathaysia Blocks, problems and tentative answers. *Journal of Southeast Asian Earth Sciences* **13**, 223–35.

CHEN, J. F., FOLAND, K. A. & ZHOU, T. X. 1985. Mesozoic granitoids of the Yangtze foldbelt, China: Isotopic constraints on the magma sources. In *The Crust – The Significance of Granites gneisses in the Lithosphere* (ed. L. R. Wu), pp. 217–37. Athens: Theophrastus Publications.

CHEN, J. F. & JAHN, B.-M. 1998. Crustal evolution of southeastern China: Nd and Sr isotopic evidence. *Tectonophysics* **284**, 101–33.

CHEN, J. F., ZHOU, T. X. & FOLAND, K. A. 1985. $^{40}$Ar–$^{39}$Ar and Rb–Sr geochronology the Qingyang batholith, Anhui Province, China. *Geochemistry* **4**(3), 220–35.

CHEN, J. F., ZHOU, T. X., LI, X. M., FOLAND, K. A., HUANG, C. Y. & LU, W. 1993. Sr and Nd isotopic constraints on source regions of the intermediate and acid intrusions from southern Anhui Province. *Geochimica* **3**, 261–8.

CHERNIAK, D. J. & WATSON, E. B. 2000. Pb diffusion in zircon. *Chemical Geology* **172**, 5–24.

CLEMENS, J. D. 2003. S-type granitic magmas – petrogenetic issues, models and evidence. *Earth Science Reviews* **61**, 1–18.

GEISLER, T., PIDGEON, R. T., KURTZ, R., VAN BRONSWIJK, W. & SCHLEICHER, H. 2003*a*. Experimental hydrothermal alteration of partially metamict zircon. *American Mineralogist* **88**, 1496–1513.

GEISLER, T., RASHWAN, A. A., RAHN, M. K. W., POLLER, U., ZWINGMANN, H., PIDGEON, R. T., SCHLEICHER, H. & TOMASHEK, F. 2003*b*. Low-temperature hydrothermal alteration of natural metamict zircons from the Eastern Desert, Egypt. *Mineralogical Magazine* **67**, 485–508.

GEISLER, T., ULONSKA, M., SCHLEICHER, H., PIDGEON, R. T. & VAN BRONSWIJK, W. 2001. Leaching and differential recrystallization of metamict zircon under experimental hydrothermal conditions. *Contributions to Mineralogy and Petrology* **141**, 53–65.

GENG, H. Y., XU, X. S., O'REILLY, S. Y., ZHAO, M. & SUN, T. 2006. Cretaceous volcanic-intrusive magmatism in western Guangdong and its geological significance. *Science in China (Series D)* **49**(7), 696–713.

GRIFFIN, W. L., BELOUSOVA, E. A., SHEE, S. R., PEARSON, N. J. & O'REILLY, S. Y. 2004. Archean crustal evolution in the northern Yilgarn Craton: U–Pb and Hf-isotope evidence from detrital zircons. *Precambrian Research* **131**(3–4), 231–82.

GRIMMER, J. C., RATSCHBACHER, L., MCWILLIAMS, M., FRANZ, L., GAITZSCH, I., TICHOMIROWA, W., HACKER, B. R. & ZHANG, Y. 2003. When did the ultrahigh-pressure rocks reach the surface? A $^{207}$Pb/$^{206}$Pb zircon, $^{40}$Ar–$^{39}$Ar white mica, Si-in-white mica, single-grain provenance study of Dabie Shan synorogenic foreland sediments. *Chemical Geology* **197**, 87–110.

HOFMANN, A. W., JOCHUM, K. P., SEUFERT, M. & WHITE, W. M. 1986. Nb and Pb in oceanic basalts: new constraints on mantle evolution. *Earth and Planetary Science Letters* **79**, 33–45.

HOSKIN, P. W. O. 2005. Trace-element composition of hydrothermal zircon and the alteration of Hadean zircon from the Jack Hills, Australia. *Geochimica et Cosmochimica Acta* **69**, 637–48.

JACKSON, S. E., PEARSON, N. J., GRIFFIN, W. L. & BELOUSOVA, E. A. 2004. The application of laser

ablation–inductively coupled plasma–mass spectrometry to in situ U–Pb zircon geochronology. *Chemical Geology* **211**, 47–69.

JIANG, S. Y., YU, J. M. & LU, J. J. 2004. Trace and rare-earth element geochemistry in tourmaline and cassiterite from the Yunlong tin deposit, Yunnan, China: implication for migmatitic–hydrothermal fluid evolution and ore genesis. *Chemical Geology* **209**, 193–213.

LI, W. X. & ZHOU, X. M. 2000. Geochemical constraints on the petrogenesis of Late Mesozoic igneous rocks in coastal area of Zhejiang and Fujian Province. *Progress in Natural Science* **10**(7), 630–41.

LI, Z. X. 1998. Tectonic history of the major East Asian lithospheric blocks since the mid-Proterozoic – A Synthesis. In *Mantle dynamics and plate interactions in East Asia* (eds M. Flower, S. L. Chung, C. H. Lo & Y. Y. Lee), pp. 221–43. American Geophysical Union, Geodynamics Series no. 27. Washington, DC.

LING, H. F., ZHAI, J. P. & ZHANG, B. T. 1990. Genesis of rapakivi feldspar and dark-coloured enclaves of the Yaocun granite body in southern Anhui. *Geological Review* **36**, 20–30 (in Chinese with English abstract).

LUDWIG, K. R. 2001. *ISOPLOT 2.49: A Geochronological Toolkit for Microsoft Excel*. Berkeley Geochronology Centre Special Publication, vol. 1a. University of California at Berkeley, 58 pp.

MARTIN, L., DUCHÊNE, S., DELOULE, E. & VANDERHAEGHE, O. 2006. The isotopic composition of zircon and garnet: a record of the metamorphic history of Naxos, Greece. *Lithos* **87**, 174–92.

MCDONOUGH, W. F. & SUN, S. S. 1995. The composition of the Earth. *Chemical Geology* **120**, 223–53.

NORMAN, M. D., PEARSON, N. J., SHARMA, A. & GRIFFIN, W. L. 1996. Quantitative analysis of trace elements in geological materials by laser ablation ICP-MS: instrumental operating conditions and calibration values of NIST glasses. *Geostandards Newsletter* **20**, 247–61.

NORMAN, M. D., GRIFFIN, W. L., PEARSON, N. J., GARCIA, M. O. & O'REILLY, S. Y. 1998. Quantitative analysis of trace element abundances in glasses and minerals: a comparison of laser ablation inductively coupled plasma mass spectrometry, solution inductively coupled plasma mass spectrometry, proton microprobe and electron microprobe data. *Journal of Analytical Atomic Spectrometry* **13**, 477–82.

PELLETER, E., CHEILLETZ, A., GASQUET, D., MOUTTAQI, A., ANNICH, M., HAKOUR, A. E., DELOULE, E. & FERAUD, G. 2007. Hydrothermal zircons: A tool for ion microprobe U–Pb dating of gold mineralization (Tamlalt–Menhouhou gold deposit – Morocco). *Chemical Geology* **245**, 135–61.

PITCHER, W. S. 1997. *The Nature and Origin of Granite*. Second edition. London: Chapman & Hall, 387 pp.

RIZVANOVA, N. G., LEVCHENKOV, O. A., BELOUS, A. E., BEZMEN, N. I., MASLENIKOV, A. N., KOMAROV, A. N., MAKEEV, A. F. & LEVSKIY, L. K. 2000. Zircon reaction and stability of the U–Pb isotope system during interaction with carbonate fluid: experimental hydrothermal study. *Contributions to Mineralogy and Petrology* **139**, 101–14.

SHEN, W. Z., LING, H. F. & SUN, T. 2007. Sr–Nd isotope geochemistry of Late Mesozoic granite and volcanic rocks, SE China. In *The Genesis of Late Mesozoic Granites and Lithosphere Geodynamic Evolution* (ed. X. M. Zhou), pp. 123–60. Beijing: Science Press.

SUN, W. D., DING, X., HU, Y. H. & LI, X. H. 2007. The golden transformation of the Cretaceous plate subduction in the west Pacific. *Earth and Planetary Science Letters* **262**, 533–42.

SUZUKI, K. & ADACHI, M. 1991. Precambrian provenance and Silurian metamorphism of the Tsubonosawa paragneiss in the South Kitakami terrane, Northeast Japan, revealed by the chemical Th–U–total Pb isochron ages of monazite, zircon and xenotime. *Geochemical Journal* **25**, 357–76.

SUZUKI, K., ADACHI, M. & YAMAMOTO, K. 1990. Possible effects of grain-boundary REE on the REE distribution in felsic melts derived by partial melting. *Geochemical Journal* **24**, 57–74.

SUZUKI, K. & KATO, T. 2008. CHIME dating of monazite, xenotime, zircon and polycrase: protocol, pitfalls and chemical criterion of possibly discordant age data. *Gondwana Research* **14**, 569–86.

VAN ACHTERBERGH, E., RYAN, C. G., JACKSON, S. E. & GRIFFIN, W. L. 2001. Data reduction software for LA–ICP–MS: appendix. In *Laser Ablation–ICP–Mass Spectrometry in the Earth Sciences* (ed. P. J. Sylvester), pp. 239–43. Principles and Applications, Mineralogical Association of Canada (MAC) Short Course Series, Ottawa, Ontario, Canada.

WANG, D. Z., LIU, C. S. & PENG, Y. M. 1965. *Jiuhuashan intrusions, Anhui Province*. Geological Department of Nanjing University, Research Report of National Science and Technology (in Chinese).

WANG, X. X., WANG, T., JAHN, B. M., HU, N. G. & CHEN, W. 2007. Tectonic significance of Late Triassic post-collisional lamprophyre dykes from the Qinling Mountains (China). *Geological Magazine* **144**, 1–12.

WU, C. L., ZHOU, X. R., HUANG, X. C., ZHANG, C. H. & HUANG, W. M. 1996. $^{40}Ar$–$^{39}Ar$ chronology of intrusive rocks from Tongling. *Acta Petrologica Mineralogica* **15**, 299–306 (in Chinese with English abstract).

XIE, X., XU, X. S., XING, G. F. & ZOU, H. B. 2003. Geochemistry and genesis of Early Cretaceous volcanic rock assemblages in eastern Zhejiang. *Acta Petrologica Sinica* **19**(3), 385–98 (in Chinese with English abstract).

XU, X. S., DONG, C. W., LI, W. X. & ZHOU, X. M. 1999. Late Mesozoic intrusive complexes in coastal area of Fujian, SE China: The significance of the gabbro–diorite–granite association. *Lithos* **46**, 299–315.

YAN, J., CHEN, J. F. & XU, X. S. 2008. Geochemistry of Cretaceous mafic rocks from the lower Yangtze region, eastern China: Characteristics and evolution of the lithospheric mantle. *Journal of Asian Earth Sciences* **33**, 177–93.

YAN, J., LIU, H. Q., SONG, C. Z., XU, X. S., AN, Y. J., LIU, J. & DAI, L. Q. 2009. Zircon U-Pb geochronology of the volcanic rocks from Fanchang-Ningwu volcanic basins in the Lower Yangtze region and its geological implications. *Chinese Science Bulletin* **54**(16), 2895–2904.

YUAN, F., ZHOU, T. F., FAN, Y., YUE, S. C., ZHU, G. & HOU, M. J. 2006. Characteristics of Nd–Sr isotopes of the Yanshanian magmatic rocks in the Jiangnan rise bordering Anhui and Jiangxi provinces. *Chinese Journal of Geology* **41**(1), 133–42.

YUAN, F., ZHOU, T. F., YUE, S. C., ZHU, G. & HOU, M. J. 2003. Rare earths of magmatic rocks of Yanshanian stage in adjacent region of Anhui and Jiangxi Provinces, Jiangnan uplift. *Journal of the Chinese Rare Earth Society* **21**(5), 600–3.

ZHANG, G. W., BAI, Y. B., SUN, Y., GUO, A. L., ZHOU, D. W. & LI, T. H. 1985. Composition and evolution of the Archaean crust in central Henan, China. *Precambrian Research* **27**, 7–35.

https://doi.org/10.1017/S0016756809990367 Published online by Cambridge University Press

ZHANG, G. W., YU, Z. P., DONG, Y. P. & YAO, A. P. 2000. On Precambrian framework and evolution of the Qinling belt. *Acta Petrologica Sinica* **16**, 11–21 (in Chinese with English abstract).

ZHOU, X. M. & LI, W. X. 2000. Origin of Late Mesozoic igneous rocks of Southeastern China: implications for lithosphere subduction and underplating of mafic magmas. *Tectonophysics* **326**, 269–87.

ZHOU, X. M., SUN, T., SHEN, W. Z., SHU, L. S. & NIU, Y. L. 2006. Petrogenesis of Mesozoic granitoids and volcanic rocks in South China: a response to tectonic evolution. *Episodes* **29**, 26–33.

https://doi.org/10.1017/S0016756809990367 Published online by Cambridge University Press